Materials Chemistry and Physics 115 (2009) 209–216

Contents lists available at ScienceDirect

Materials Chemistry and Physics

journal homepage: www.elsevier.com/locate/matchemphys

Synergistic catalysis effect in pentanol conversion into di-*n*-pentyl ether on ZSM-5 supported titania catalysts synthesized by sol–gel

Mohamed Mokhtar Mohamed [a,*], M.M. Al-Esaimi [b]

[a] *Faculty of Science, Chemistry Department, Benha University, Benha 11764, Egypt*
[b] *Faculty of Applied Science, Chemistry Department, Umm Al-Qura University, Makkah, Saudia Arabia*

ARTICLE INFO

Article history:
Received 9 June 2008
Received in revised form
18 November 2008
Accepted 18 November 2008

Keywords:
1-Pentanol
Di-*n*-pentyl ether
Ti/ZSM-5
Sol–gel
Characterization

ABSTRACT

The synthesis of TiZSM-5 (TiZ) catalysts using acid catalyzed sol–gel method via different molar ratios of tetra-isopropyl orthotitanate [Ti(O-i-Pr)$_4$] was thoroughly characterized by inductively coupled plasma optical emission (ICP-OE), X-ray diffraction (XRD), particle size analyzer, N_2 adsorption, pyridine-FTIR and ultra-violet visible (UV–vis) spectroscopy. Liquid phase dehydration of 1-pentanol to di-*n*-pentyl ether (DNPE) was tested for the catalysts. Characterization of TiZSM-5 catalysts clearly shows that at low loadings (up to 5 wt%) titanium atoms were on the inner surface of zeolite layers mainly in tetrahedral environment as conceived from UV–vis (248–260 nm) and IR (960 and 1123 cm^{-1}) results besides surface texturing data that showed lower surface areas (524–480 m^2 g^{-1}) and pore volumes (0.4955–0.4530 cm^3 g^{-1}) as compared to the parent (587 m^2 g^{-1} and 0.5642 cm^3 g^{-1}). A distortion of tetrahedral Ti species was perceived at high-titania loadings (≥10 wt%) evidencing its existence on zeolite surfaces as a distinctive anatase phase. The catalytic dehydration of 1-pentanol over 5, 10 and 15 wt% TiZ catalysts achieved 70% conversion and 10TiZ showed the highest selectivity (60%) to DNPE. This was due to enhancing Brönsted acid sites, retaining crystallinity, decreased particles size and to the relatively large BET surface area. The effect of temperature (298–523 K), time (4–16 h), titania loadings (2.5–15 wt%) as well as solvent engagement on the selectivity to DNPE was thoroughly investigated. The nano-sized TiO_2 crystals in/on 10TiZ surfaces and zeolite pore volume seem to provide excellent possibilities for diffusion of reactants and products, which of significant importance in heterogeneous catalysis.

1. Introduction

Titanium dioxide has attracted much attention due to its promising applications in the environmental photocatalytic degradation of large organic pollutants in wastewater [1–4]. Titania is an important catalytic material, not only because of its effectiveness in photo-assisted reactions [5–7] but also when used as a catalyst support for transition metal oxides. Several methods have been cited in the literature indicating the way of increasing the specific surface area of titania and thermal stability of the anatase phase [8]. One of these ways is the incorporation of TiO_2 into zeolites structure for the purpose of making use of involved acid–base properties and oxidation–reduction chemistry that could be altered by the preparation conditions. The application of zeolitic materials such as H-ZSM-5 [9,10] and X and Y Faujasites [11–13] in both protonated and indigenous alkali forms in alcohol dehydration has been reported, however, transition metal exchanged zeolites have by comparison received considerable attention in the literature. The balance between acidic and basic functions in alkali exchanged zeolites is known due to their significant impact in organic rearrangement reactions [14–16].

The catalytic dehydration of alcohols to the respective ethers and/or alkenes is assuming increasing importance as a synthetic methodology. Ethers; as one of the products, are also highly desirable commodities as oxygenate fuel additives [17,18]. Ballantine et al. [19] studied the liquid phase dehydration of alcohols (at 473 K) over montmorillonite catalysts and concluded that primary alcohols underwent preferential intermolecular dehydration to yield dialkyl ethers in high yields while secondary alcohol favored the formation of alkene via a facile intramolecular dehydration pathway. The conversion of both methanol and ethanol [20,21] over alumina yielded dialkyl ether (and water) as the major product(s) where an increase in reaction temperature induced alkene formation. The consensus of opinion is that, over solid catalysts, lower reaction temperatures (373–423 K) favor the formation of the ether while the alkene is preferred at high temperatures (>423 K). Zeolite catalysts have a much larger tendency to retain (or to readsorb) olefins in the pores in the form of oligomerization products. Ideally, a high-efficiency catalyst designed for the alcohol dehydration/coupling reactions would possess strong Brönsted acid sites [22] in close

* Corresponding author.
E-mail address: mohmok2000@yahoo.com (M.M. Mohamed).

0254-0584/$ – see front matter © 2008 Elsevier B.V. All rights reserved.
doi:10.1016/j.matchemphys.2008.11.057

proximity to one another on a thermally stable, high-surface area support with low-diffusion resistance to the reactants and products.

Titanium phosphates have been tested for alcohols dehydration and some of the results are contradictory since the behavior of the catalyst depended to a great deal on preparation details [23]. Titanium phosphates with lamellar structure give rather dimethyl ether (DME) and methane as products of methanol conversion [24] but dimethyl ether also became a desired product as DME makes an ultra clean alternative fuel for engines with emission levels meeting guaranteed standards [25].

Diesel fuel properties are constantly being analyzed in an attempt to further reduce fuel emissions including hydrocarbons, CO, NOx, unburned hydrocarbons and smokes. There are many options, most often refinement processes or improving the cetane number. Essentially, short and branched ethers (used in gasoline) have a good octane number but poor cetane number, while those ethers used in diesel are linear and have a comparatively long chains (ideally nine or more carbons). Di-*n*-pentyl ether (DNPE) has shown most effective in reducing emissions, and is also relatively simple to synthesize via the bimolecular dehydration of 1-pentanol on acid catalysts. It is commonly believed that isolated Ti in the framework of the TS-1 zeolite; denoted as Ti–O–Si, is the active site of some selective reactions. Therefore, we report the sol–gel synthesis of Ti-ZSM-5 catalysts and their characterizations by infrared spectroscopy (IR), UV–vis, X-ray diffraction (XRD), particle size analyzer, ICP, pyridine-FTIR, surface texturing and their use as solid catalysts; for the first time, for pentanol dehydration from the liquid phase.

2. Experimental

2.1. Catalyst preparation

The preparation of TiO_2/NaZSM-5 was carried out using acid catalyzed sol–gel technique. 7.4 ml of Ti(O-i-Pr)$_4$ (Aldrich, 97%) was poured dropwise onto 20 ml of 1 M HNO_3 whilst stirring to achieve colloidal suspension of Ti oxide covered by hydroxides as follows:

$$Ti(iso\text{-}OC_3H_7)_4 + H_2O \rightarrow (OC_3H_7)_3Ti\text{–}OH + C_3H_7OH \quad (1)$$

$$2(OC_3H_7)_3Ti\text{–}OH \rightarrow (OC_3H_7)_3Ti\text{–}O\text{–}Ti(OC_3H_7)_3 + H_2O \quad (2)$$

$$(OC_3H_7)_3Ti\text{–}OH + C_3H_7OTi(OC_3H_7)_3 \rightarrow (OC_3H_7)_3Ti\text{–}O\text{–}Ti(OC_3H_7) + C_3H_7OH \quad (3)$$

After complete addition, agitation for 2.0 h to give transparent TiO_2 sol was achieved. On the other hand, zeolite (NaZSM-5, SiO_2/Al_2O_3 = 300, purchased from Zeolyst International) in H_2O was left for 1 h and then mixed with a certain amount of the sol; to achieve definite loading, then left for stirring for 2 h, followed by washing and centrifugation to make supernatant neutral. The composites mixture dried for 1 h at 393 K and finally calcined at 673 K for 5 h, then stored in the dark. Samples were designated as *X*TiZ, where *X* indicates the wt% of titania. For comparison purposes, TiO_2 (P-25, mean particle size 80 nm, which is predominantly anatase (487 and 555 cm^{-1}) purchased from Degussa) was used without any treatment. It gives diagnostic hydroxyl bands at 3736, 3715, 3673 and 3663 cm^{-1} [7].

2.2. Characterization

The X-ray diffractograms of various samples were measured by using a Philips diffractometer (type PW 3710). The patterns were run with Ni-filtered copper radiation (λ = 1.5404 Å) at 30 kV and 10 mA with a scanning speed of $2\theta = 2.5^\circ$ min^{-1}. The crystallinity of the prepared samples was calculated using the ratio of the sum of the areas of the most intense peaks ($2\theta = 22–25^\circ$) of prepared samples to that of the same peaks for the parent and multiplying by 100. The instrumental line broadening was measured using a LaB6 standard [26].

Dynamic light scattering, LB-500, was used for determining particles size. Sample preparation was carried out as follows: Dispersion of 20 mg of the sample in H_2O together with sodium hexametaphosphate was stirred for 10 min. The suspension was ultrasonicated for 10 min then acquired for the measurement. Each sample was repeated three times to obtain more accurate results.

Ti ions concentration was measured by inductively coupled plasma optical emission spectroscopy using using Optima 4300 DV (ICP-OES).

FTIR spectra of the samples were recorded with a JASCO single beam FTIR 5300-spectrometer with 50 co-added scans at 2 cm^{-1} resolution. All IR measurements were carried out at room temperature using KBr disks.

UV–visible absorption spectra of the materials were obtained for the dry pressed disk samples using UV–vis spectrophotometer (Shimadzu 2101-PC) between 190–350 nm range. Absorption spectra were referenced to $BaSO_4$.

The nitrogen adsorption isotherms were measured at 77 K using a conventional volumetric apparatus. The specific surface area was obtained using the BET method. The micropore volume and the external surface area were obtained from the *t*-plot method.

Thin, but intact, self-supporting wafers (30 ± 5 mg cm^{-2}) of the adsorbents were prepared and mounted inside a specially designed, heatable and evacuable, all quartz glass IR cell. The cell containing samples, equipped with CaF_2 windows, was hooked to a Pyrex glass Gas/Vac handling system and evacuated to 10^{-5} Torr at 523 K prior subjecting to 8 Torr of pyridine vapor. A spectrum of the gas phase was recorded before a 5 min degassing of the cell (at 300 K) and taking a spectrum of the wafer plus irreversibly adsorbed pyridine. By absorption subtraction of the cell and wafer, IR difference spectra of the gas phase and Py adsorbed species were obtained, respectively. Quantitative determination of Lewis and Brönsted acid sites was based on using identical sample discs in all experiments including weight, homogeneity and thickness.

The catalytic dehydration of pentan-1-ol took place in a tubular stainless steel reactor that fitted with a threaded cap and a PTFE seal and immersed into an oil bath temperature-controlled at the required temperature. A weighed amount of the catalyst (0.1 g) was loaded into the reactor into which 34 mmol of pentan-1-ol was included. Shaking of the components was performed; at the required temperature, inside the oil bath all the time before carrying out the measurements. After the desired heating period, the reactor was removed from the oil bath and quenched directly in cold water. The products of the reaction were analyzed quantitatively by gas chromatography (GC) using a SRI 8310 Gas chromatograph, equipped with a flame ionization detector (FID). A 17′ × 1/8″ stainless steel column packed with 10% Carbowax 20 M on Chromosorb PAW (120–140 mesh) was used for the separation of reaction products. Helium gas was used as carrier gas at a flow rate of 20 cm^3 min^{-1}. The oven temperature was maintained at 413 K with the injector and detector held at 473 K. The injection volumes for the quantitative analyses were 1.0 μl. The calibration of the sensitivity of reactants and products for GC was done by the comparison with standard compounds purchased commercially. Each run was made three times to comprehend with no doubt the reproducibility of the catalytic tests. This emphasizes that both the type reaction system and operation mode are very rigorous.

3. Results and discussion

3.1. XRD and particle size

The XRD patterns of TiZ samples are shown in Fig. 1. All samples show identical patterns signifying the preserve of ZSM-5 structure even following the titanation with Ti-ISOP. A marked decrease in crystallinity was perceived following the increase in Ti loading and reached 32% (68% amorphous) for the 15TiZ sample. The anatase phase is only observed at high-TiO_2 loadings ($\geq$10 wt%) signifying characteristic peaks at $2\theta = 25.5^\circ$, 37.4°, 39.2°, 45.0° and 47.1°. Accelerating the crystallization of well-defined anatase phase starting from 10TiZ reflects the lower dispersion of TiO_2 inside zeolite channels. On the other hand, at low loadings (2.5, 5 wt%) Ti ions are either

Table 1
The ICP analysis and XRD characterization data of TiZ catalysts.

Samples	$TiO_2/TiO_2 + SiO_2$ (mol mol^{-1})	Crystallite size determined from Scherrer equation, *D* (nm)	Lattice parameters (Å)			Cell volume, *V* (Å)^3	Crystallinity (%)
			a	*b*	*c*		
ZSM-5	–	42.10	19.704	20.0472	13.71	5415.5	100
2.5TiZ	0.025	42.50	19.821	20.078	13.212	5257.9	90
5TiZ	0.05	43.50	19.87	20.162	13.312	5333.0	58
10TiZ	0.1	41.11	19.91	20.0312	13.121	5233.0	51
15TiZ	0.15	40.51	19.65	20.112	13.101	5177.5	32

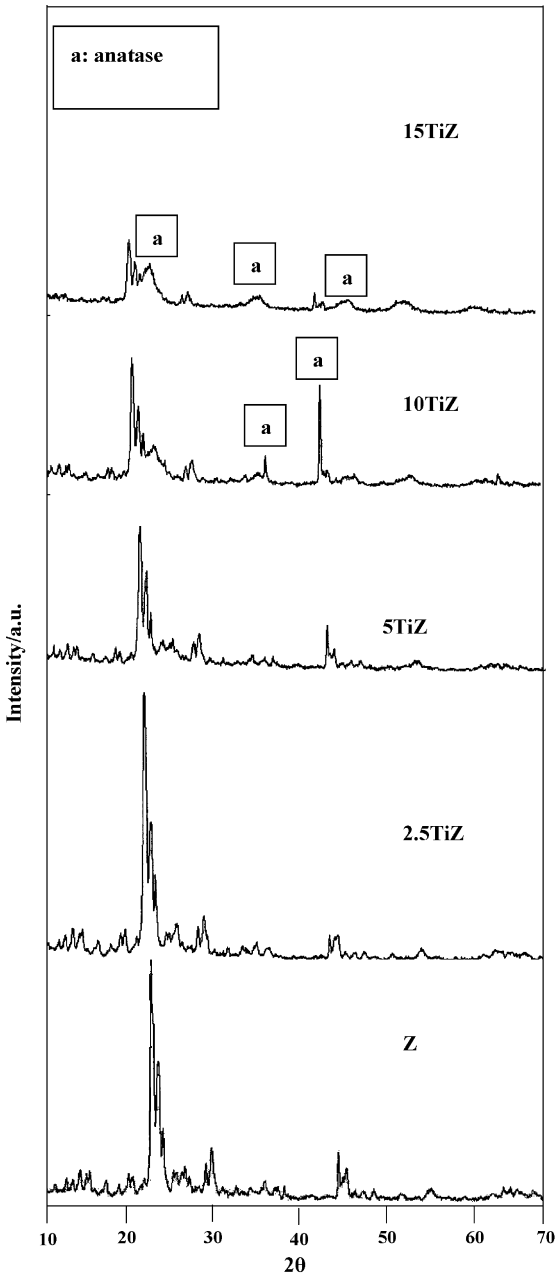

Fig. 1. XRD patterns of titania containing ZSM-5 samples.

well dispersed inside zeolite channels or they hidden as smaller crystallites of ca. 3–4 nm diameter and thus obscured to be seen due to the technique limitations. The shift of the lattice parameter *a* (Table 1) in Z (19.704 Å) into higher values in 2.5TiZ (19.821 Å), 5TiZ (19.870 Å) and 10TiZ (19.910 Å) proposes the inclusion of titania particles within zeolite linkages causing their expansions. However, this is not the case in 15TiZ that indicates a value comprises of 19.651 Å suggesting random clogging of the channels generated by aggregation of titania that intricated deterioration in the channels ordering emphasized from the relative decrease in crystallinity to 32% as compared to the parent. Concurrently, the particles size analyzer results (Fig. 2); performed without grinding, indicated a decrease in particles size as a result of increasing titania loadings probably because of the amorphism depicted for zeolite samples as a result of increasing Ti loadings. The average crystals size obtained by applying Scherrer equation (Table 1) were comparable to those estimated using the light scattering technique (Fig. 2) comprehending that most of the particles are in the form of crystals. This implies that the exhibited decrease in surface area values, reported in the coming section, is not only a result of dilution of zeolite with titania but also due to decreasing the zeolites crystallinity.

3.2. Texture properties

Textural characteristics of TiZ samples, obtained by analyzing N_2 adsorption results, are compiled in Table 2, in comparison with the Z sample. The values of BET surface area show a decrease comprises, respectively of 10.7, 18.5, 25 and 34.9% for 2.5-, 5-, 10- and 15TiZ when compared with that of the parent. Similarly, the total pore volume (V_p^{total}) suffered a decrease consists of 12.2, 19.7, 23.2 and 24.1% $cm^3\,g^{-1}$ for 2.5-, 5-, 10- and 15TiZ, respectively. Contrarily, the pore radius did not indicate significant changes. These results point to deposition of Ti species deep inside zeolite channels

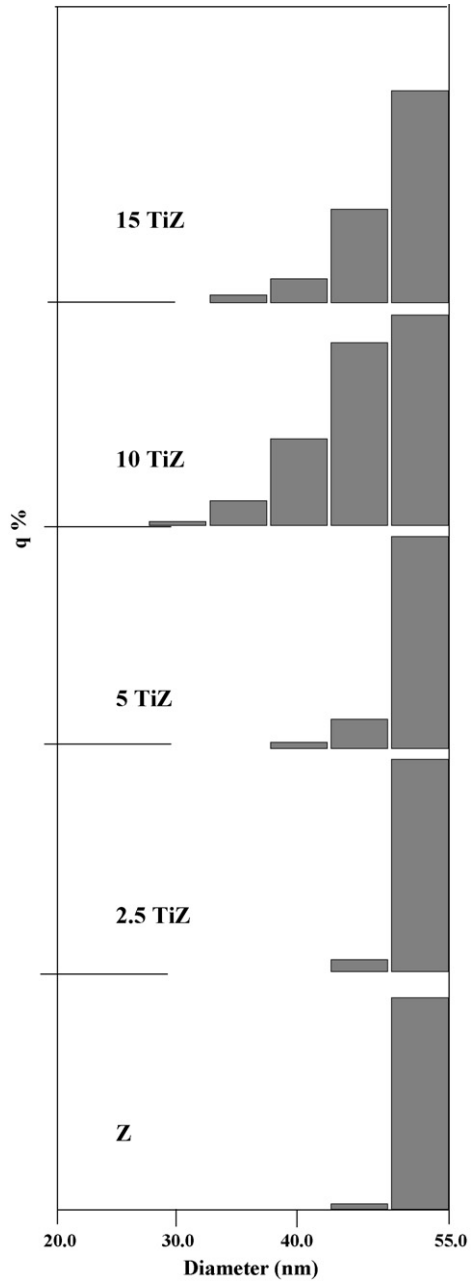

Fig. 2. Particles size distribution of titania containing ZSM-5 samples.

Table 2
Surface texturing data of TiZ catalysts.

Sample	S_{BET} ($m^2\,g^{-1}$)	S_t ($m^2\,g^{-1}$)	V_p^{total} ($cm^3\,g^{-1}$)	r^- (Å)	S^{μ} ($m^2\,g^{-1}$)	S^{ext} ($m^2\,g^{-1}$)	S^{wid} ($m^2\,g^{-1}$)	V_p^{μ} ($cm^3\,g^{-1}$)	V_p^{wid} ($cm^3\,g^{-1}$)	Microporosity (%)	C-const
ZSM-5	587	603	0.5642	24	535	58	52	0.5142	0.1205	91	95
2.5TiZ	524	495	0.4955	24	452	47	72	0.4346	0.0610	87	29
5TiZ	480	473	0.4530	24	427	42	53	0.4101	0.0429	90	19
10TiZ	440	462	0.4335	23	400	40	40	0.3879	0.0408	90	60
15TiZ	382	382	0.4285	22	320	35	62	0.3652	0.0633	90	25

S_{BET}, BET surface area; V_p, total pore volume; r^-, mean pore radius; S_t, surface area derived from V_l–t plots; S^{μ}, surface area of micropores; S^{ext}, external surface area; S^{wid}, surface area of wide pores, V_p^{μ}, volume of micropores; V_p^{wid}, volume of wide pores; $V_p^{mic}/V_p^{total} \times 100$, microporosity percentages.

affecting the pore volume that by its turn influences the samples BET surface areas. Combining the results obtained from XRD and BET investigations, one may suggest that at low loadings (up to 5 wt%) titania particles were on the inner surface of zeolite layers and thus partial blockage of the pore volume was attained. Therefore, effective changes in average surface areas; indicative of the marked dispersion of titania within zeolite channels, are obtained. According to the consequent decrease in V_p at low loadings (2.5, 5) an expected extra decline; in V_p, for 10TiZ and 15TiZ comprised of 48 and 60% instead of 23.2 and 24.1% could have been obtained. This reflects that major part of titania is attending on zeolite surface as TiO_2 anatase, at high loadings. The refinement results show that the Ti content inside the zeolite structure strongly influences unit cell parameters, so that a cation exchange can be expected and roughly can be deduced by its value, i.e. eligibility for forming Ti–O–Si linkages, as will be seen later. *t*-Plots, on the other hand, derived from adsorption data determined by the adsorption branch (type-II) of the isotherms, implementing the reference *t*-curve determined previously [27] on a non-porous silicon oxide surface (C-BET), collaborates with these conclusions. The Z sample exhibited an upward deviation (Fig. 3) indicating the presence of mesopores [28]. That deviation suffered reduction with increasing titania loadings demonstrating narrowing pore volume. The 15TiZ sample exhibited larger hysteresis loop than 10TiZ. This indicates that at such high loadings expected large amounts of Ti hydroxide complexes upon hydrolysis and crowding therein (channels) set out some of Ti particles inside the surface; as well as on it forming TiO_2 anatase, enhancing by its turn the mesoporous character of ZSM-5. As another plausible explanation, the accelerated diffusion of Ti in zeolite framework induced defect framework in the volume of zeolite particles which later form cavities in mesopore range.

3.3. FTIR and UV–vis spectra

IR spectroscopy was also used to characterize the samples (Fig. 4). There are several clear differences among TiZ samples when compared with Z. As expected, all the samples; except 15TiZ, show an intense band at 550(557) cm^{-1}; characteristics of secondary building unit, confirming the intact structure of the zeolite (MFI) even following titanation [29]. The spectrum of 2.5TiZ showed a shoulder at approximately 960 cm^{-1}, indicative of either Ti incorporation into the four-coordinate Si framework [30] or due to Si–OH groups or defect sites. However, the existence of other band at 1123 cm^{-1} eliminates the above controversial assignment concerning the 960 cm^{-1} band and rather strengthens the titania insertion into the zeolite framework [31,32]. The prominent presence of the sole band at 1088 cm^{-1} at high-Ti loadings decreases the possibilities of finding well incorporated Ti ions into framework positions; since it was originally detected in the Z sample, in agreement with XRD results. No TiO_2 anatase bands were revealed in the low-IR region [33] for all samples unlike the case in XRD technique. IR spectra of TiZ in the hydroxyl groups region exhibit differences among themselves and among the Z sample most importantly is the evolution of acidic hydroxyls at 3597 and 3629 cm^{-1} (in 2.5TiZ), 3625 cm^{-1} (in 5TiZ), 3632 cm^{-1} (in 10TiZ) and 3637 cm^{-1} (in 15TiZ) those exceedingly intensified than that positioned at 3620 cm^{-1} in Z. The evolution of new intensified OH groups is probably due to destruction of Si–O–Al linkages and formation of Ti–OH and Si(Al)–OH groups. The band at 3620 cm^{-1} is vanished in 2.5TiZ reflecting the interaction of Ti ions with acidic Brönsted sites. These sites were highly enhanced in intensity as well as in strength for 10TiZ to appear at 3632 cm^{-1}. The presence of bands at 3741 and 3743 cm^{-1} for 5- and 10TiZ are due to isolated silanol groups where that at 3711 cm^{-1} for 2.5TiZ is probably associated with terminal SiO–H groups in which oxygen interacts with the proton of a nearby hydroxyl group [34,35] or due to Ti–OH groups. The incorporation of Ti at a 15 wt% loading in TiZ sample induces the consumption of many silanol groups, as revealed by the progressive disappearance of the IR bands of SiO–H vibrations at 3758, 3650, 3510, 3459 and 3416 cm^{-1} in Z. Fig. 5 depicts the background subtracted UV–vis spectra of TiZ samples calcined at 673 K. Due to the absence of d–d transitions in the range 600–800 nm (not shown), the UV–vis bands observed at 248–260 nm for TiZ sampls were assigned to oxygen to tetrahedral Ti charge transfer transitions. The shift of the charge transfer bands to higher energy upon increasing Ti loading into 15% (248 nm), coupled with the simultaneous decrease of their intensities, indicated a greater distortion of tetrahedral zeolite structures; as evidenced previously from IR and XRD investigations. The absence of bands in the 300–350 nm region for both 10- and 15TiZ samples presumes the dispersity of external framework titania species (anatase TiO_2). This is because the blue shift of the spectrum (from 260 to 248 nm for 15TiZ) is usually indicative for decreasing the particle size and the confinement of highly dispersed TiO_2 nanoparticles [36]. This indicates that TiO_2 ions are mostly dispersed inside zeolite surfaces.

3.4. Pyridine adsorption

Fig. 6 shows the infrared spectra of pyridine adsorbed; at 298 K, on TiZ samples followed by brief outgassing (0.5 h) at the same temperature for avoiding physisorbed pyridine molecules. Bands at 1444 and 1541 cm^{-1} are found in the spectrum of Z sample attributed, respectively, to pyridine bound to Lewis and Brönsted acid sites. The 1444(1446) cm^{-1} band showed a significant decrease in intensity in 2.5TiZ proposing a marked decrease in Lewis acidity. On 5TiZ and 10TiZ, bands at 1544(1555) and 1639(1644) cm^{-1}, indicative of Brönsted acidity, are displayed. In addition, 5TiZ shows bands at 1588 and 1573 cm^{-1} due to δN^+–H vibrations [37] signifying the increase of Brönsted acidity on this particular sample. Outgassing the sample up to 423 K resulted in an increase in the Brönsted acid sites for 2.5-, 5- and 10TiZ samples as presented in Table 3. This increase in Brönsted acidity is also expected to result from partial exchange of Na^+ cations of ZSM-5 during its dissolution. Wide distribution of acid sites for TiZ samples and existence of sites with high-Brönsted acid strength was obtained on increasing the evacuation temperature into 423 K. Contrarily, 2.5TiZ showed a decrease in Brönsted acid strength with temperature revolving a different state of Ti atoms as compared with rest of samples.

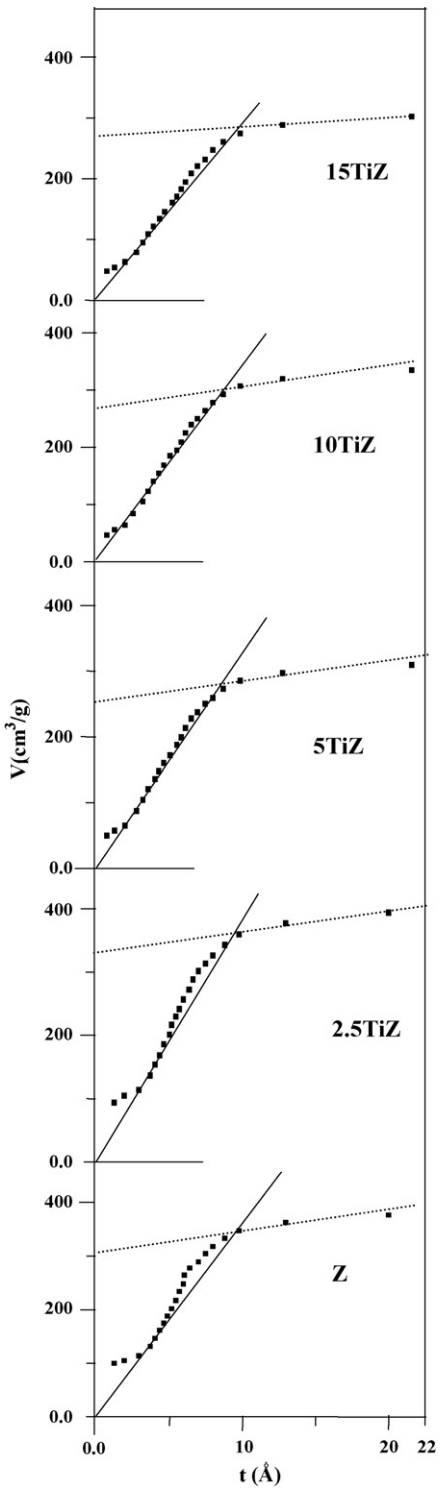

Fig. 3. V_l–t plots of titania containing ZSM-5 samples.

3.5. Liquid-phase catalysis

The reaction envisaged in this study was the heterogeneous dehydration of 1-pentanol over TiZ catalysts. 1-Pentanol may undergo either a bimolecular dehydration to di-*n*-pentyl ether (DNPE) or a monomolecular dehydration to pentenes. The formation of alkenes involves a protonation of the alcohol by the surface Brönsted acid sites through a slow dissociation into a carbonium ion and a fast expulsion of the hydronium ion into the alkene.

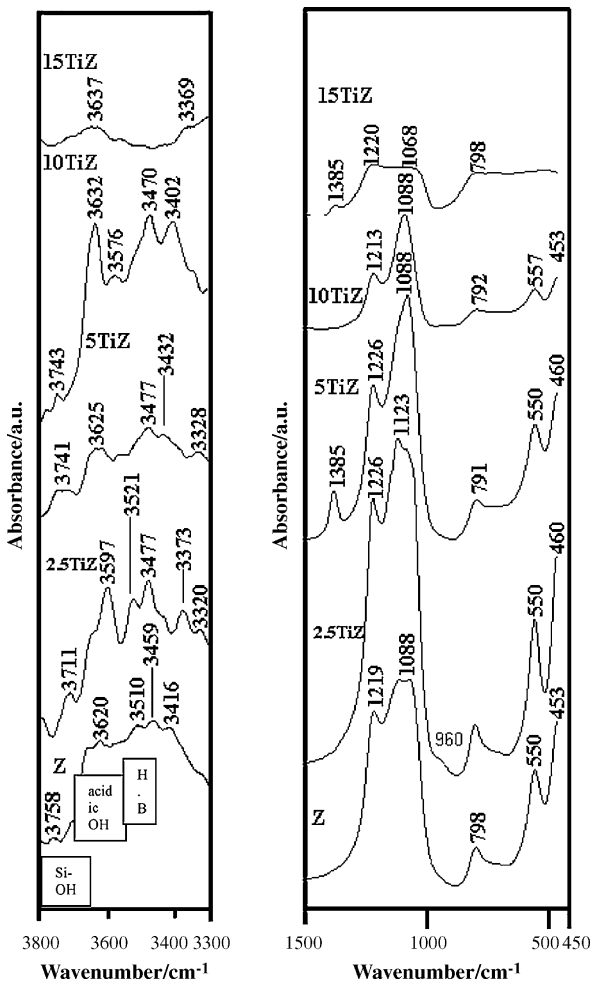

Fig. 4. FTIR spectra of titania containing ZSM-5 samples in the low (450–1500 cm^{-1}) and high (3300–3800 cm^{-1}) IR regions.

In dehydration reactions for the isomeric form of the alkene to predominate, and from a consideration of reaction equilibrium constants [38], pent-2-ene is the thermodynamically preferred isomer. The generation of pentyl ether is the result of a condensation reaction involving from the standard point of conventional organic chemistry [39], nucleophilic substitution with the protonated alcohol on substrate and the second pentan-1-ol molecule

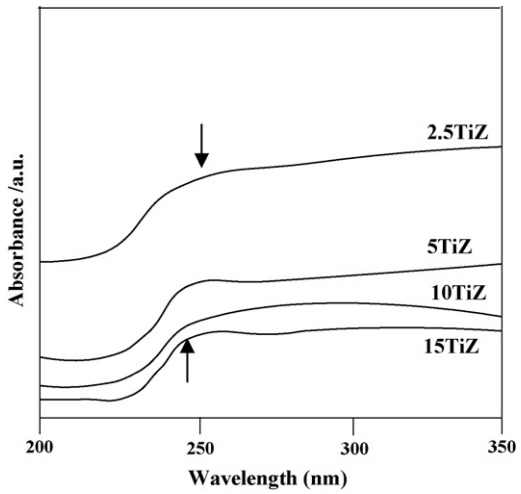

Fig. 5. UV–vis spectra of titania containing ZSM-5 samples.

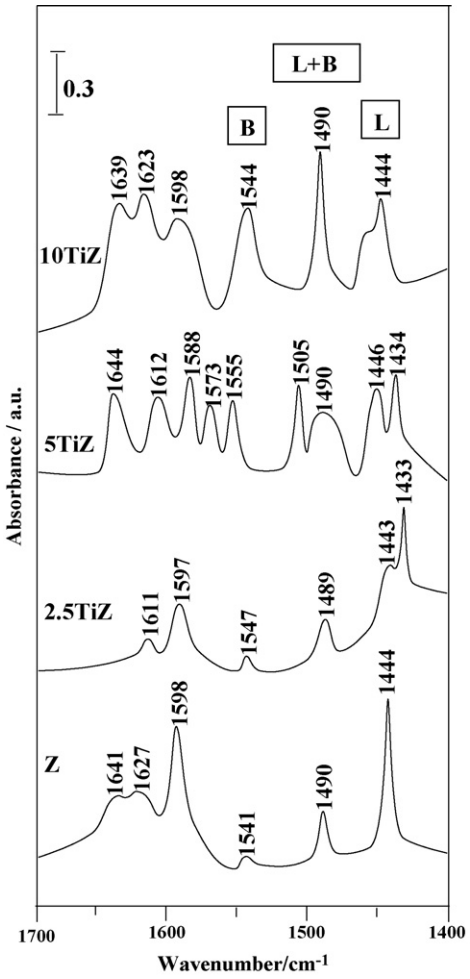

Fig. 6. FTIR spectra of pyridine adsorbed; at room temperature, on titania containing ZSM-5 samples following evacuation at the same temperature for 0.5 h.

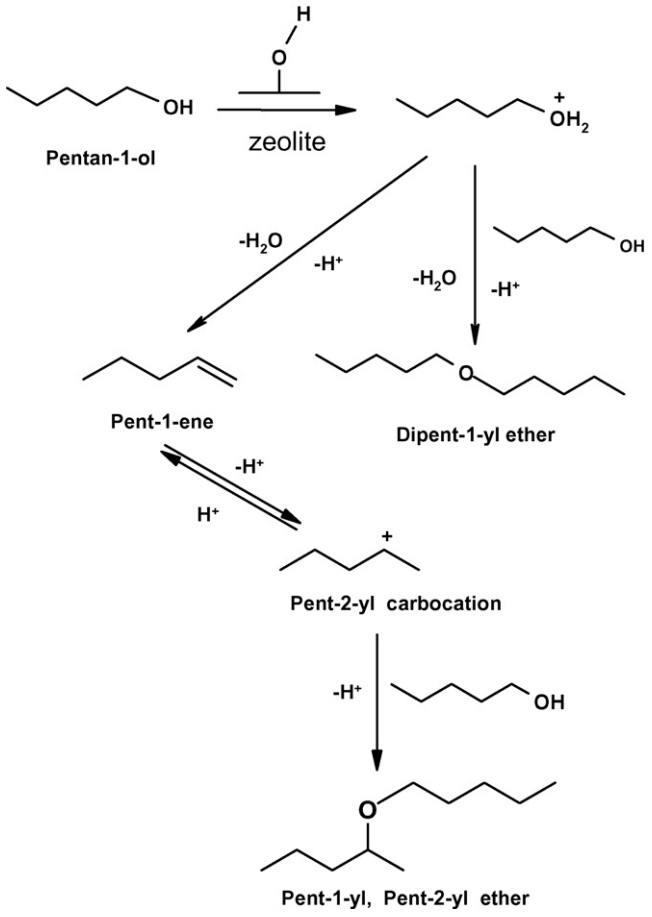

Scheme 1. The pentan-1-ol dehydration.

as the nucleophile. For simplification Scheme 1 shows the reaction mechanism of 1-pentanol dehydration.

The conversion dehydration of pentanol over 2.5-, 5-, 10- and 15TiZ materials and selectivities towards ether and 1-pentene (including minor amounts of *cis* and *trans*-pent-2-ene) are shown in Fig. 7. The rate of conversion was almost comparable for 5-, 10- and 15TiZ catalysts achieving 70% where ether selectivity was the highest for the 2.5TiZ sample (63%) that showed the lowest conversion (6.4%). This lowest conversion could be due to mass transfer limitations of reacting species as a result of involving Ti–O bonds of longer bond distance (0.182 nm) than that of Si–O (0.160 nm). In addition, increasing Brönsted acid sites density (2.04, Table 3) might decrease strong absorption sites for pentanol on zeolite surfaces. For comparison purposes, titanium free Z sample indicates conversion of 1.9% revolving the decisive advantage of titania contaning samples. The TiO_2 P-25 sample, on the other hand, offered

Table 3
Quantitative results of acidic sites for TiZ materials as assessed by Py adsorption with varying temperatures.

Sample	Temperature (K)	Number of sites (μmol g^{-1})		
		[L]	[B]	[B]/[L][a]
ZSM-5	298	39.8	1.14	0.029
2.5TiZ		3.7	7.54	2.04
5TiZ		23.0	8.10	0.35
10TiZ		45.8	39.3	0.86
ZSM-5	373	81.0	3.1	0.038
2.5TiZ		90.5	4.9	0.054
5TiZ		13.1	10.2	0.78
10TiZ		38.5	38.1	0.99
ZSM-5	423	82.5	2.6	0.032
2.5TiZ		21.5	7.6	0.35
5TiZ		7.3	8.0	1.10
10TiZ		24.3	45.0	1.85

[a] B/L ratio: Brönsted to Lewis sites concentration that obtained by dividing Pyridine quantities.

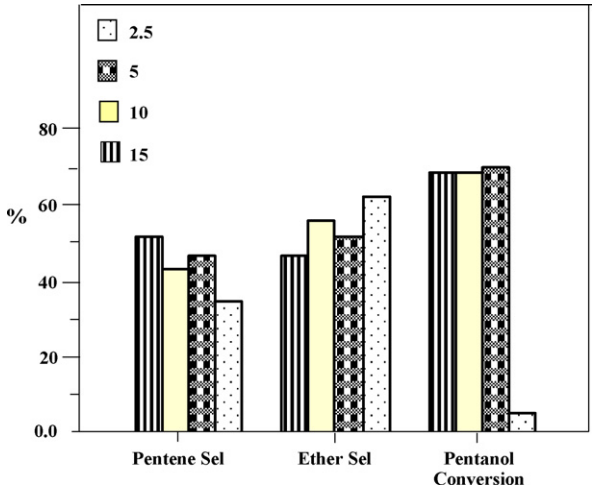

Fig. 7. Effect of titania loading in TiZ samples on the activity (conversion and selectivity) towards 1-pentanol dehydration at 453 K for 4 h.

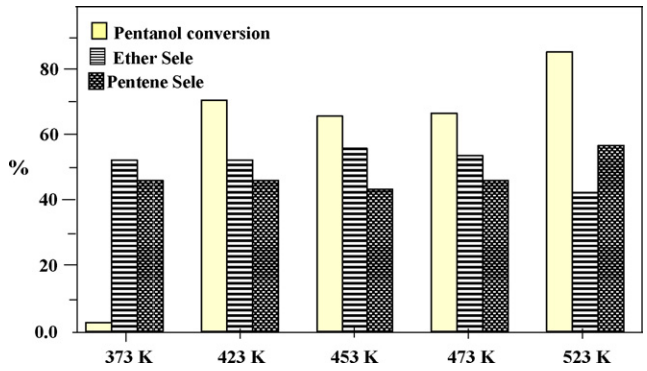

Fig. 8. Dependence of activity (conversion and selectivity) percentages in pentanol dehydration on temperature for the 10TiZ catalyst (at constant time 4 h).

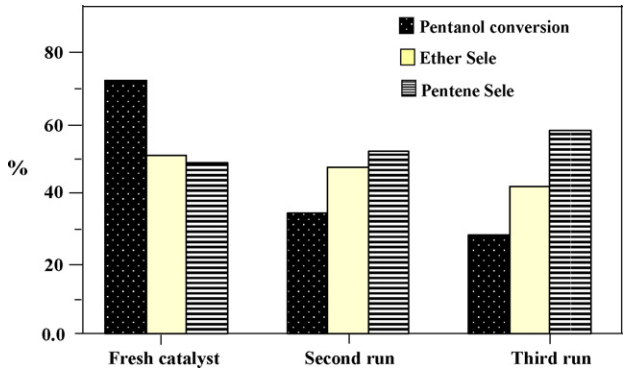

Fig. 10. Dependence of activity (conversion and selectivity) percentages in pentanol dehydration on re-using the 10TiZ catalyst for three consecutive runs at 453 K for 4 h.

conversion of 4.8% emphasizing the significance of the synergistic effect of both Ti and ZSM-5. The 10TiZ sample showed the highest selectivity; following the 2.5TiZ sample, comprised of 60% and thus taken as a representative for the incoming studies. Increasing the molar atomic ratios of $TiO_2/TiO_2 + SiO_2$ beyond 0.1 (Table 1) decreases the activity. The 10TiZ sample showed that the rate of conversion is shifted towards high values (85%) upon increasing the temperatures into 523 K (Fig. 8) but on the other hand, selectivities to DNPE are reduced (43.3%) to be lower than pentenes (56.7%). It has been acknowledged that selectivity of catalysts towards ether requires simultaneous adsorption of alcohol molecules on two active centers close enough to each other [40]. Thus, the decrease in di-*n*-pentyl ether (DNPE) with temperatures exceeding 473 K in favor of pentenes is a result of decomposing the formed ether to produce pentenes and alcohol those by turn may give branched ethers or addition reaction thereof producing additional alkenes and water, by intermolecular dehydration of alcohols [41,42]. This indeed can be due to increasing Brönsted acid sites with temperatures (Table 3) together with their strength, i.e. dipentyl ether is dehydrated to pentenes at sites of increasing affinity of Brönsted acidity. Going beyond the boiling point of DNPE (453 K) by further 40 K reduces markedly the etherification reaction.

The degree of conversion was more or less similar for all catalysts (~70%) with 16 h reaction time. The degree of selectivity towards pentenes was observed to slightly decline with time as shown in Fig. 9. Exceeding DNPE selectivity over pentenes as a result of increasing contact time predicts that the former is not only produced from isomerization of 1-pentene but also directly from pentanol [42]. These experiments indicate that the dehydration of pentanol at such high conversions takes place most probably

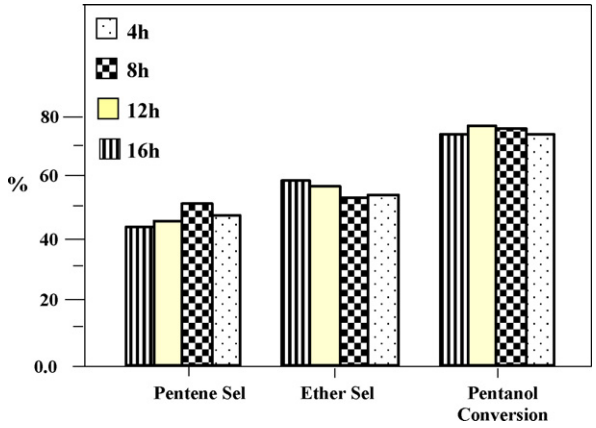

Fig. 9. Dependence of activity (conversion and selectivity) percentages in pentanol dehydration on time at 453 K for the 10TiZ catalyst.

on the inner surface of the catalysts rather than on the outer surface that represents ~10% of the total surface area. It appears favorable to use small zeolite crystals as for 10TiZ since mass transfer limitations are of less importance. Furthermore, deactivation is expected to proceed in a slow rate on small crystals due to their large surface areas.

To shed an idea on the effect of recycling on catalyst activity, Fig. 10 showed deactivation of the fresh catalyst after performing first three runs using the 10TiZ catalyst. That test was carried out on the recovered catalyst following centrifugation and drying at 323 K for 24 h. Following the third run the conversion value of 30% was obtained. Similarly, the degree of selectivity towards ether showed a significant decrease from 52 to 44%. On the other hand, the selectivity towards pentenes showed an enhancement from 50% on the fresh catalyst into 59% following the third run. Indeed, the formation of carbonaceous deposits on the catalyst surfaces mask active sites available for condensation products. As it is known, alkenes produced from primary alcohols have a tendency to polymerize and form cokes on sites of stronger acidity and this makes them unsuitable for further testing [25]. In addition, prohibiting intracrystalline diffusion of DNPE from 10TiZ might occur owing to the repulsion and attraction between sorbed reactants and products species and the crystals surface. For such small crystals the surface resistance can exceed the intracrystalline diffusional resistance by several orders of magnitude. Thus, an additional regeneration step was carried out for the same catalyst by calcining at 673 K for 12 h. It showed an increase in conversion into 57% without significant loss in selectivities to ether (55%) and pentenes (45%). No leached Ti was detected by ICP; after the first run, indicating that its a heterogeneously catalyzed reaction and, however, the activity loss might be due to poisoning by deposited carbons.

The catalytic dehydration of 1-octanol on the same catalyst gives by comparison lower activity (conversion 30%, ether selectivity 6%) probably because of steric factors concerning octanol moieties and their adsorption on near by active sites hindering etherification reaction to take place properly and instead higher concentration of unidentified products was produced.

Using solvents such as CCl_4 and benzene while catalyzing pentanol reaction indicate decreased activities probably due to competitive adsorption between solvents and pentanol and thus the number of active sites available for reactants are diminished. The conversion is decreased from 69% on 10TiZ into 57% when using benzene and the selectivity to DNPE was only 17% where in the case of CCl_4 a conversion comprises of 59% was depicted with a selectivity of 52% to DNPE. This indicates that the presence of Cl^- in the reaction media resulted most likely via degradation with TiO_2 inhibit active sites on TiZ catalyst through their adsorption but indeed still higher in activity than when using benzene. This

probably due to the higher absorbability of TiZ samples towards benzene rather than CCl_4.

4. Conclusions

TiZSM-5 catalysts prepared by sol–gel method exhibited high activity in 1-pentanol dehydration yielding large amounts of DNPE at selectivity comprised of 60% and conversion equal 70%. A mixture of pentene isomers together with DNPE was found to vary with temperature, time and titania contents in the sense that DNPE decreases with temperature increase beyond 473 K and increases with contact time and titania loadings (till 10 wt%). This was explained in the view that TiZ interaction influences the quantity of the incorporated titania and the type of the formed Ti acid sites. It has been proved that incorporated Ti preferentially in tetrahedral T sites together with those of highly dispersed TiO_2 species are active sites for DNPE formation. It was also shown that the catalytic activity towards DNPE is increasing with medium Brönsted acidity and BET surface areas together with decreasing particles size. The last two parameters provided excellent possibilities for diffusion of DNPE without resistance. The catalytic activity of TiZ catalysts was largely depends on the interaction of the reactants with the adsorption sites of the zeolite; such as hydroxyl groups and Brönsted sites, then extended onto the TiO_2 sites producing high-catalytic reactivities.

References

[1] H.H. King, in: B. Delmon, J.T. Yates (Eds.), Transition Metal Oxides: Surface Chemistry & Catalysis, Elsevier, Amsterdam, 1989, p. 1.
[2] M.S. Wainwright, N.R. Foster, Catal. Rev. 19 (1979) 211.
[3] M.A. Vannice, J. Catal. 44 (1982) 199.
[4] K.N.P. Kumar, Appl. Catal. A 119 (1994) 163.
[5] R. Kozlowski, R.F. Pettifer, J.M. Thomas, J. Phys. Chem. 87 (1983) 5176.
[6] M.M. Mohamed, T.M. Salama, T. Yamaguchi, Coll. Surf. A 207 (2002) 25.
[7] M.M. Mohamed, Appl. Catal. A 267 (2004) 135;
M.M. Mohamed, I. Othman, R.M. Mohamed, J. Photochem. Photobiol. A 191 (2–3) (2007) 153.
[8] M. Raimondo, G. Perez, A. De Stefains, A.A.G. Tomlinson, Appl. Catal. A 250 (2003) 187.
[9] J. Topp-Jorgense, US patent 4,536,485 (1985) to Holdon Topsoe A/S, Denmark.
[10] T. Takeguchi, K. Yanagisawa, T. Inui, M. Inoue, Appl. Catal. A 192 (2000) 201.
[11] F.S. Stone, A.L. Agudo, Z. Phys. Chem. 64 (1969) 161.
[12] S.J. Gentry, R. Rudham, J. Chem. Soc., Faraday Trans. I 70 (1974) 1685.
[13] P.A. Jacob, M. Tielen, J.B. Uytterhoeven, J. Catal. 50 (1977) 98.
[14] A. Heidekum, M.A. Harmer, W.F. Holderich, J. Catal. 188 (1999) 230.
[15] R.A. Sheldon, J.A. Elings, S.K. Lee, H.E.B. Lempers, R.S. Downing, J. Mol. Catal. A 134 (1998) 129.
[16] I. Othman, R.M. Mohamed, I.A. Ibrahim, M.M. Mohamed, Appl. Catal. A 299 (2006) 95;
D. Barthomeuf, Catal. Rev. 38 (1996) 521.
[17] W. Turek, J. Haber, A. Krowiak, Appl. Surf. Sci. 252 (2005) 823.
[18] J. Tejero, F. Cunill, M. Iborra, J.F. Izquierdo, C. Fite, J. Mol. Catal. A 182–183 (2002) 541.
[19] J.A. Ballantine, M. Davis, I. Patel, J.H. Purnell, M. Rayanakorn, K.J. Williams, J.M. Thomas, J. Mol. Catal. 26 (1984) 37.
[20] B.C. Gates, W. Rodriguez, J. Catal. 31 (1973) 27.
[21] R. Thornton, B.C. Gates, J. Catal. 34 (1974) 275.
[22] M.M. Mohamed, F. Abd El-Hai, J. Mol. Catal. A 211 (2004) 199.
[23] L.G.A. Vande Water, J.C. Vand der Waal, J.C. Jansen, T. Maschmeyer, J. Catal. 223 (2004) 170.
[24] J.H. Kim, M.J. Park, S.J. Kim, O.S. Joo, K.D. Jung, Appl. Catal. A 264 (2004) 37.
[25] A. Ludmany, S.S. Kurek, A. Stoklosa, G. Wilczynski, A. Wojtowicz, J. Zajecki, Appl. Catal. A 267 (2004) 149.
[26] J.I. Langford, J.C. Wilson, J. Appl. Cryst. 11 (1978) 102.
[27] M.D. Remy, G. Poncelet, J. Phys. Chem. 99 (1995) 773.
[28] P. Trens, J.W. Peckett, V.N. Stathopoulos, M.J. Hudson, J. Pomonis, Appl. Catal. A 241 (2003) 217.
[29] M.M. Mohamed, T.M. Salama, J. Coll. Interf. Sci. 249 (2002) 104.
[30] M. Liu, X. Guo, X. Wang, C.-H. Liang, C. Li, Catal. Today 93–95 (2004) 659.
[31] M.M. Mohamed, W.A. Baumy, M. Khairy, M.A. Mousa, Micropor. Mesopor. Mater. 97 (2006) 66.
[32] M. Takeuchi, T. Kimura, M. Hidaka, D. Rakhmawaty, M. Anpo, J. Catal. 246 (2007) 235.
[33] J.R. Sohn, S.H. Lee, Appl. Catal. A 266 (2004) 89.
[34] M.A. Anderson, M.-J. Gieselman, Q.J. Xu, Membr. Sci. 39 (1988) 243.
[35] F. Haque, E. Vaisman, C.H. Langford, A. Kantzas, J. Photochem. Photobiol. A: Chem. 169 (2005) 21.
[36] A. Tuel, L.G. Hubert-Pfalzgraf, J. Catal. 217 (2003) 343.
[37] M.W. Urban, Vibrational Spectroscopy of Molecules and Macromolecules on Surfaces, Wiley, Chichester, 1993, pp. 171–185.
[38] S.G. Lias, J.F. Liebman, R.D. Levin, S.A. Kafafi, NIST Standard Reference Data Base 25, Structure & Properties, Version 2.01, 1994.
[39] W.H. Brown, Organic Chemistry, Saunders, New York, 1995.
[40] M. Klimenkov, S.A. Nepijko, W. Ratz, X. Bao, J. Cryst. Growth 231 (2001) 577.
[41] J. Tejero, C. Fite, M. Iborra, J.F. Izquierdo, R. Bringue, F. Cunill, Appl. Catal. 308 (2006) 223.
[42] F. Cunill, J. Tejero, C. Fite, M. Iborra, J.F. Izquierdo, Ind. Eng. Chem. Res. 44 (2005) 318.